ACADEMIA ROMÂNĂ
Revue Roumaine de Chimie
http://web.icf.ro/rrch/

Rev. Roum. Chim.,
2013, *58*(4-5), 335-345

Dedicated to Professor Eugen Segal
on the occasion of his 80th anniversary

THERMAL BEHAVIOR OF ZnO PRECURSOR POWDERS OBTAINED FROM AQUEOUS SOLUTIONS

Susana MIHAIU,[a] János MADARÁSZ,[b] György POKOL,[b] Imre Miklós SZILÁGYI,[c] Tímea KASZÁS,[b] Oana Cătălina MOCIOIU,[a,*] Irina ATKINSON,[a,*] Alexandra TOADER,[a] Cornel MUNTEANU,[a] Virgil Emanuel MARINESCU[d] and Maria ZAHARESCU,[a]

[a] "Ilie Murgulescu" Institute of Physical Chemistry, Romanian Academy, 202 Splaiul Independenței, 060021 Bucharest, Roumania
[b] Department of Inorganic and Analytical Chemistry, Budapest University of Technology and Economics, H-1521 Budapest, Szt. Gellért tér 4, Hungary
[c] MTA-BME Technical Analytical Chemistry Research Group of the Hungarian Academy of Sciences, Budapest University of Technology and Economics, Department of Inorganic and Analytical Chemistry, H-1111 Budapest, Szt. Gellért tér 4, Hungary
[d] National Institute for R&D in Electrical Engineering ICPE-CA 313 Splaiul Unirii, 030138 Bucharest, Roumania

Received December 20, 2012

The formation mechanism of ZnO nanopowders was investigated by appropriate experimental methods. The studied samples have been obtained using a wet chemical route based on $Zn(NO_3)_2.nH_2O$ (ZAH) - $(CH_2)_6N_4$ (HMTA) system in which the molar ratio of the components was 4:1 and 2:1. From the same solution, depending on the experimental conditions used, gels, precipitates or hydrothermally grown powders were obtained. Thermal decomposition of the as-prepared powders was analysed by simultaneous thermogravimetric and differential-thermal analysis (TG/DTA) and differential scanning calorimetry (DSC) methods. X-ray diffraction method (XRD), FT-IR Spectroscopy and Scanning Electron Microscopy (SEM) were used to study the structure and morphology of the obtained samples and their evolution with thermal treatment. The correlation between the preparation parameters and the properties of the resulted ZnO powders was established.

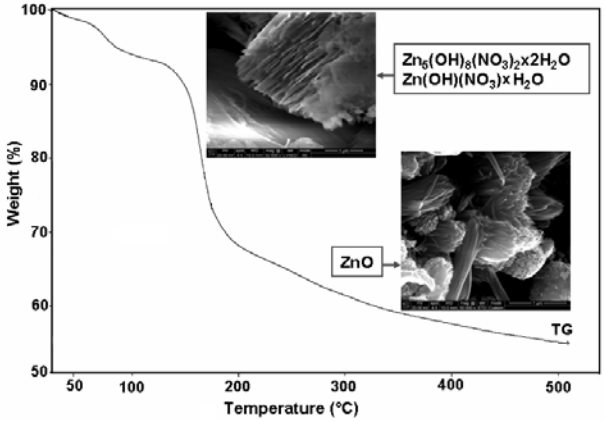

INTRODUCTION

Nanostructured ZnO materials have received considerable interest from scientists due to their remarkable performances in electronics, optics and photonics, being used as dye sensitized solar cells,[1,2] photocatalyst,[3-6] gas sensors.[7,8] The different methods such as chemical vapor deposition,[9] physical vapor deposition,[10] sonication,[11] microwave heating,[12] combustion synthesis,[13] sol–gel processes,[14] hydrothermal/solvothermal methods,[15-17] homogeneous precipitation[18, 19] and electrochemical method[20] were used for synthesis of ZnO nanostructures. Among the above methods, the solution chemical routes become a promising option for large-scale production, which is simpler, faster and less expensive.

* Corresponding authors: oana.mocioiu@yahoo.com or irinaatkinson@yahoo.com

Table 1

Experimental condition for the precursor solution preparation

Precursor solutions	Concentration of zinc ions (Mol)	ZAH/HMTA	Reaction temperature (C^o)	Reaction time (min)	Post-reaction treatment
S1	0.1	4/1	25	120	Gelling 90 days and drying gels at 85°C, 48 h
S2	0.1	4/1	60	120	
S3	0.05	2/1	85	120	non
S4	0.05	2/1	25	15	Hydrothermal 90°C, 12 h

$Zn(NO_3)_2{\cdot}nH_2O$(ZAH)-hexamethylenetetramine (HMTA) system has been reported in recent years for ZnO powders preparation.[21-23] It is generally considered as a very simple and novel process. The understanding the growth mechanism of varieties of morphologies of ZnO still needs further improvement. On the basis of the previous results of other researchers[24] and of our own data, the growth process of ZnO crystallites in the mentioned system is generally accepted *via* the following mechanism:

$$(CH_2)_6N_4 + 6H_2O \rightarrow 6HCHO + 4NH_3 \quad (1)$$

$$NH_3 + H_2O \rightarrow NH_4^+ + OH^- \quad (2)$$

$$Zn^{2+} + NH_3 \rightarrow Zn(NH_3)^{2+}_4 \quad (3)$$

$$Zn(NH_3)^{2+}_4 + 4OH^- \rightarrow Zn(OH)^{2-}_4 + 4NH_3 \quad (4)$$

$$Zn^{2+} + 4OH^- \rightarrow Zn(OH)^{2-}_4 \quad (5)$$

$$Zn(OH)^{2-}_4 \rightarrow ZnO + H_2O + 2OH^- \quad (6)$$

In the present work the formation mechanism of ZnO nanopowders was investigated using a wet chemical route based on ZAH-HTMA system in which the molar ratio of the components was 4:1 and 2:1. The solution with 2:1 molar ratio was used also for obtaining ZnO powders by hydrothermal method and the results obtained by chemical and hydrothermal method were compared.

EXPERIMENTAL

The starting reagents (reagent grade) for the precursor solutions preparation were zinc nitrate tetrahydrate-$Zn(NO_3)_2{\cdot}4H_2O$ (ZAH) (Merck,) hexamethylenetetramine-$(CH_2)_6N_4$ (HMTA) (Merck) and deionized water.

Experimental conditions for obtaining precursor solutions were presented in Table 1.

The molar ratio ZAH:HMTA = 4:1 or 2:1 was selected in order to limit the formaldehyde formation as a consequence of HMTA decomposition.

After completion of reactions in the conditions presented in Table 1, the solutions S1 and S2 were stored at room temperature. After 90 day of storage the gelation of the solutions occurred. A supplementary drying of the obtained gels at 85°C for 42 h led to their transformation into powders. The corresponding powders were named P1 and P2.

In the experimental conditions mentioned in Table 1, solution S3 precipitates, leading directly to the powder P3.

The solution S4 was used for hydrothermal synthesis of the ZnO powders in Teflon autoclave. The autoclave was kept in a conventional laboratory oven at a constant temperature of 90°C for 12 h. After the reaction, the as-prepared powder (namely $P_{HT\ unw}$) was washed with deionized water and dried in air at room temperature to remove residual salts and organic materials ($P_{HT\ w}$ sample).

The thermal evolution of the zinc oxide precursor powders in the 20-500°C temperature range was studied by simultaneous thermogravimetric and differential thermal analysis (TG/DTA) with a STD 2960 Simultaneous DTA–TGA (TA Instruments Inc., USA) apparatus, at a heating rate of 10 °C/min, (in sealed Al crucibles with a pinhole on the top, for samples P1 and P2), with a Mettler Toledo TGA/SDTA 851^e equipment, at a heating rate of 5 °C/min, and with DSC Mettler Toledo 823e.

Gels and powders were investigated by FT-IR Spectroscopy with a Nicolet 6700 apparatus in 400-4000 cm^{-1} domain.

The XRD patterns were collected by means of a Rigaku diffractometer type Ultima IV in parallel-beam geometry. The X-ray from a Cu tube (λ=0.15418 nm) operating at 40 kV and 30 mA. Counts were collected from 10^o to 80^o with a step size of 0.02 and a speed of 5^o/min. Phase identification and Rietveld analysis were performed using Rigaku's PDXL software, with Whole Pattern Powder Fitting (WPPF) method, connected to ICDD PDF-2 database. The shift axial displacement model of the peak shift correction function was applied. The fitting was performed using the split-pseudo Voigt function and the B-spline background model. The crystallite size *D*, were estimated using Williamson -Hall approach. Phase identification of samples P1 and P2 were carried out with an X'pert Pro MPD (PANalytical Bv., The Netherland) diffractometer.

The morphology of the sample was investigated by scanning electron microscopy (SEM) using a high-resolution microscope, FEI Quanta 3D FEG model, at an accelerating voltage of 20 kV. Sample preparation was minimal and consisted in immobilizing the sample particles on a double-sided carbon tape, with no coating.

RESULTS AND DISCUSSION

1. Reagents characterization

For ZnO nanostructured powders preparation by wet chemical method, the used reagent as Zn

source was $Zn(NO_3)_2.4H_2O$. The structure of the $Zn(NO_3)_2.4(H_2O)$ (JCPDS file No.00-36-2061) is monoclinic (space group $P21/n$)[25] and is isotypic with $[Mn(H_2O)_4](NO_3)_2$.[26] However, XRD investigation is very difficult to be done due to its very high hygroscopic character. In the same time information about the thermal behavior of $Zn(NO_3)_2.4H_2O$ are reported only in helium atmosphere, probably, due to the fact that at about 50°C it dissolves in its hydration water or melts.[27]

Due to the facts mentioned above the characterization of precursors was realized by FT-IR spectroscopy and the results are presented in Table 2. The assignment of the registered vibration bands was realized based on the literature data[27, 28] and are in good agreement with the previously reported ones.

The thermal TG, DTG, and DTA curves of the starting zinc nitrate hydrate sample in air are presented in Fig. 1 and the corresponding thermal effects are summarized in Table 3.

Table 2

Main group frequencies in infrared spectra and the assignations

Frequencies in the IR spectra (cm^{-1})		Assignment
$Zn(NO_3)_2 4H_2O$	HMTA	
451		ν (Zn-O)
721		ν (N-O-)
	513, 672, 811	ν (C-C)
829		ν (N-O) in nitrates
	998, 1235	ν (C-N) in amine
1352, 1384		ν (N-O) in nitrates
1621,1763	1628	N (O-H) in H_2O
	2872, 2959	ν (C-H)
3443	3325, 3462	Overlapping bands of
		ν (C-H)
		ν (N-H)
		ν (O-H)

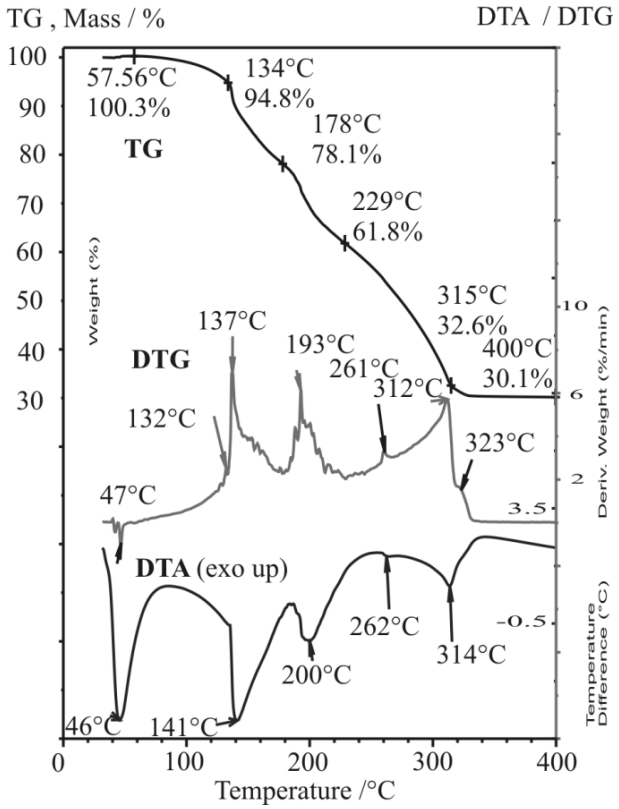

Fig. 1 – Simultaneous TG, DTG, and DTA curves of the starting zinc nitrate hydrate sample (heating rate 10 °C/min, an air flow rate 130 mL/min, sample size 35.39 mg, sealed Al crucible with a pinhole on the top).

Table 3

Thermal analysis of the starting compounds

Sample	Thermal effects (ºC)		Mass variation (%)			Assignments [26]
	endo	exo	Temperature range (ºC)	Calc.	Exp.	
$Zn(NO_3)\cdot 4H_2O$	46		20- 47	-	no	Melting
	141		47-133		94.8	Water evolution
			133-178		78.1	Nitrate decomposition
			178-229	62.1	61.1	$Zn(OH)(NO_3).H_2O$
	200		229-266	49.5	52..3	$Zn(NO_3)_2.2Zn(OH)_2$
	262		266-321	31.1	30.1	ZnO
	314		321-500			Combustion of organic residue
$(CH_2)_6N_4$ (HMTA)		281	184-350		0.0099	Combustion

The sharp endothermic peak seen on DTA curve at about 46 ºC is connected to the melting of zinc nitrate tetrahydrat, being consistent with the thermodynamic data. [26]

The other effects are connected to the water evolution and the reagent decomposition. Correlating the experimental data with the calculated ones it could be concluded that the decomposition takes place by formation of intermediate hydroxylated Zn nitrate and mixed Zn nitrate and Zn hydroxide compound.

2. Powders characterization

a) Powders obtained by chemical methods

As resulted from the experimental part, the solutions with the same initial composition behave differently in different experimental conditions.

If the solution of ZAH:HMTA with 4:1 molar ratio, was reacted and stored at low temperatures, gels were obtained. By drying at 48 h at 80^{o}C the gels transform into powders and samples P1 and P2 result.

If for the solution of ZAH:HMTA with the molar ratio 2:1 the reaction takes place at high temperature (85^{o}C), powder resulted directly from synthesis (sample P3).

The hydrothermal treatment of the solution of ZAH:HMTA with molar ratio 2:1 produces powder like sample (P_{HT}).

The important aspect that should be investigated is the structure of the obtained powders in different experimental conditions and their thermal behavior in order to transform the precursor powders in ZnO.

The X-ray diffraction patterns (not presented here) of the P1 and P2 powders have shown that the main crystalline compounds identified were $Zn(OH)(NO_3)(H_2O)$ (JCPDS file No. 04-011-3473) and NH_4NO_3 (JCPDS file No. 00-008-0452).

The X-ray diffraction pattern of the P3 powder is presented in Fig. 2 and shows the presence of the same zinc hydroxide nitrate hydrate, as in the case of the P1 and P2 samples, beside the penta-zinc octahydroxide compound. The phase composition and the crystallites size determined from the XRD data for the P3 powder are presented in Table 4.

The structure of $Zn_5(OH)_8(NO_3)_2.2H_2O$ consists of infinite brucite-like layers, with one quarter of octahedrally coordinated zinc atoms replaced by tetrahedrally coordinated zinc atoms located below and above the plane. $Zn(OH)NO_3.H_2O$ is not layered and consists of infinite double chains of edge sharing octahedra, in which zinc coordinates three hydroxyls, one nitrate anion and two water molecules.[29]

Table 4

Phase composition and crystallite size of sample P3

Phase name	Content (%)	Crystallite size (Å)
Pentazinc octahydroxide bis(nitrate(V))	53.0(8)	164.53(9)
Zinc hydroxide nitrate hydrate	47.0(10)	107.90(7)

FT-IR spectrum of the P3 powder (Fig. 3) contains OH stretching vibrations of the layer hydroxyls and water molecules in the region 3660–2900 cm^{-1} with the upper limit corresponding to free OH groups and the lower limit to OH groups involved in significant hydrogen bonding.[29]

The absorption bands at 1633 cm^{-1} (bending vibrations of the interlayer water molecules), 1384 cm^{-1} (asymmetric stretching of N-O bond in nitrate) and 832 cm^{-1} (the symmetric stretching of N-O in nitrate) are assigned by Biswick *et al* [29] to the presence of $Zn_5(OH)_8(NO_3)_2.2H_2O$ (penta-zinc octahydroxide). For the $Zn(OH)(NO_3).H_2O$ compound characteristic set of stretching vibrations attributed to nitrate anion appears at 1335 and 1050 cm^{-1}. The vibration of O-Zn-O bonds in solid state at 744 cm^{-1} was reported in paper.[30] The characteristic bands at 521, 467 and 431cm^{-1} were attributed to the ν (Zn-O) vibrations. FTIR spectrum of the P3 powder is in good agreement with the results obtained by X-Ray diffraction investigations.

The simultaneous TG/DTA curves of the P1 and P2 samples in air are presented in Fig. 4 and the corresponding thermal effects are summarized in Table 5.

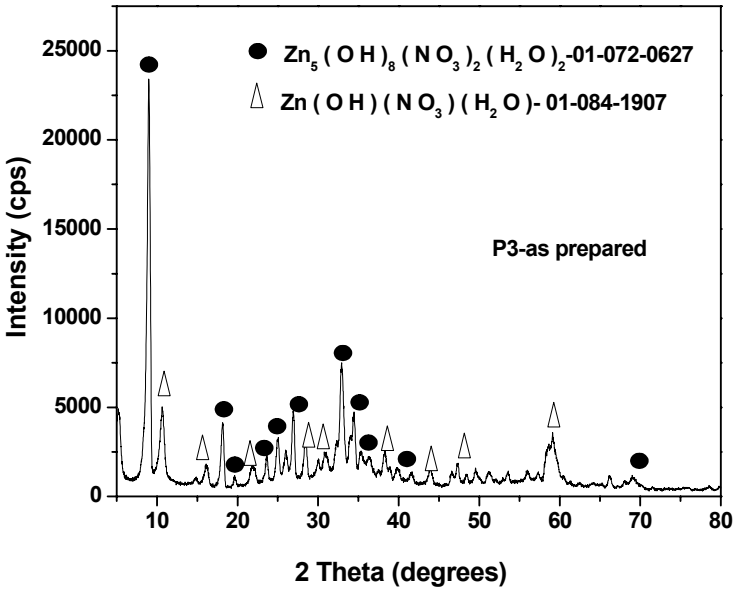

Fig. 2 – X-ray diffraction pattern of the P3 sample.

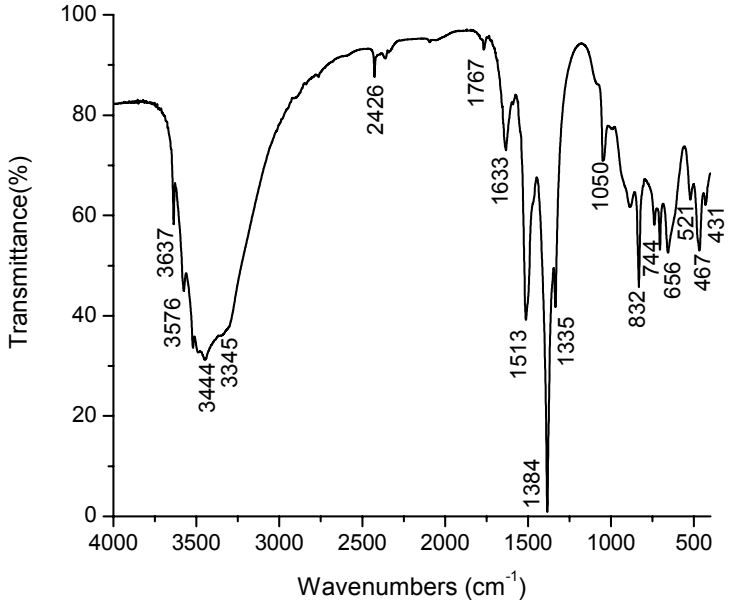

Fig. 3 – FTIR spectrum of the P3 sample.

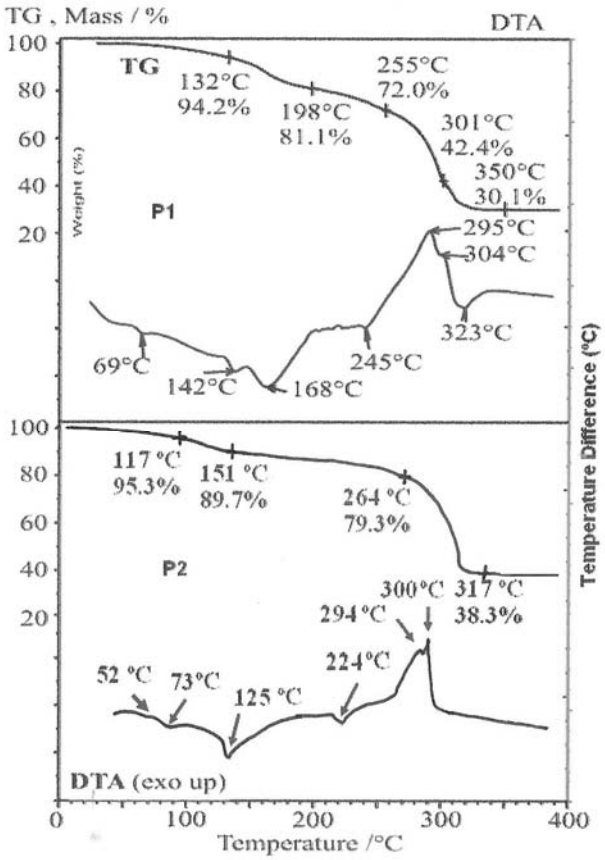

Fig. 4 – DTA/TG analysis of the P1 and P2 samples.

Table 5

Mass variation of the studied gels

Sample	Phases by XRD	Thermal effects (ºC)		Mass variation (%)	
		Endo	exo	Temperature range (ºC)	Exp.
P1	$Zn(OH)(NO_3)(H_2O)$ and NH_4NO_3	69 142 168 245	 299 304	20-132 132-187 187-255 255-301 301-400	94.2 82.1 72.0 42.4 30.1
P2	$Zn(OH)(NO_3)(H_2O)$ and NH_4NO_3	73 125 224	 291 299	20-117 117-151 151-264 264-500	95.3 89.7 79.3 38.4
P3	$Zn_5(OH)_8(NO_3)_2.2H_2O$ $Zn(OH)(NO_3).H_2O$			20- 76 76-164 164-500	95 77 55

The TG curves of the P1 and P2 samples show, more or less, a similarly behavior. The mass loss is greater in the case of P1 sample probably due to higher amount of partially reacted or residual organic components (precursor solution was obtained at room temperature). TG curves show several temperature regions for both samples which initially contain $Zn(OH)(NO_3)(H_2O)$ (Zinc hydroxide nitrate hydrate), NH_4NO_3 (ammonium nitrate), and more or less amount of organic gelly materials, respectively.

Aufredic and Louër[31] reported that $Zn(OH)NO_3.H_2O$ compound decomposes to ZnO in a two-step process via a $Zn_3(OH)_4(NO_3)_2$ phase. Malecka *et al.*[26] observed from TG analysis that $Zn_3(OH)_4(NO_3)_2$ decomposes to ZnO in two steps. They proposed, therefore, that the first decomposition step of $Zn_3(OH)_4(NO_3)_2$ involved the formation of amorphous anhydrous zinc nitrate, which then decomposed to ZnO in the second step.

In the case of the P3 sample which consists from a mixture of penta-zinc octahydroxide and zinc hydroxide nitrate (V) the mass loss is smaller than for P1 and P2 samples, respectively, due to the fact that the residual compounds were removed by washing of the obtained powder with hot water.

Literature data[31] reported that the transformation of penta-zinc octahydroxide in ZnO occurs through intermediate stages with formation of the compounds most likely as following:

$$Zn_5(OH)_8(NO_3)_2{\cdot}2H_2O \xrightarrow{80-120^\circ C} Zn_5(OH)_8(NO_3)_2 + 2H_2O \quad (7)$$

$$Zn_5(OH)_8(NO_3)_2 \xrightarrow{120-140^\circ C} Zn_3(OH)_4(NO_3)_2 + 2ZnO + 2H_2O \quad (8)$$

$$Zn_3(OH)_4(NO_3)_2 \xrightarrow{140-170^\circ C} 3ZnO + 2HNO_3 + H_2O \quad (9)$$

The temperature differences between our results and those reported in literature could be due to higher heating rate in our case.

According to the TG/DTA results the samples were isothermally treated at 300 ºC for 1 h.

In Fig. 5 the XRD pattern of the $P3_{TT}$ is presented. All the diffraction peaks can be well indexed to the hexagonal phase of ZnO with wurtzite structure and the lattice parameters determined by XRD were a=b=3.2520Å and c=5.207Å. All diffraction data were in good agreement with JCPDS files No.00-36-1451 (a = 3.24982 Å and c =5.20661 Å). No other phases were detected, and the reflections were sharp, which indicated a good crystallization of ZnO. The average crystalline size (D) of the ZnO of 184 Å was calculated using Williamson-Hall approach.

The FT-IR spectrum of $P3_{TT}$ (Fig. 6) presented one intense band at 460 cm^{-1} assigned to Zn-O vibration. The weak and broad bands at 840 cm^{-1}(N-O symmetric stretch), 1383 cm^{-1} (N-O asymmetric stretch), 1559 cm^{-1} (H_2O vibration) and 3435 cm^{-1} (O-H bond) were probably species absorbed on the surface of powder.

SEM images of P3 sample (which consists of a mixture of penta-zinc octahydroxide and zinc hydroxide nitrate) and $P3_{TT}$ sample (which consists of only one zinc oxide phase) show similar blade-like nanostructures (Fig.s 7). This fact points out that the initial blade-like structure is kept even after thermal treatment at 300 ºC.

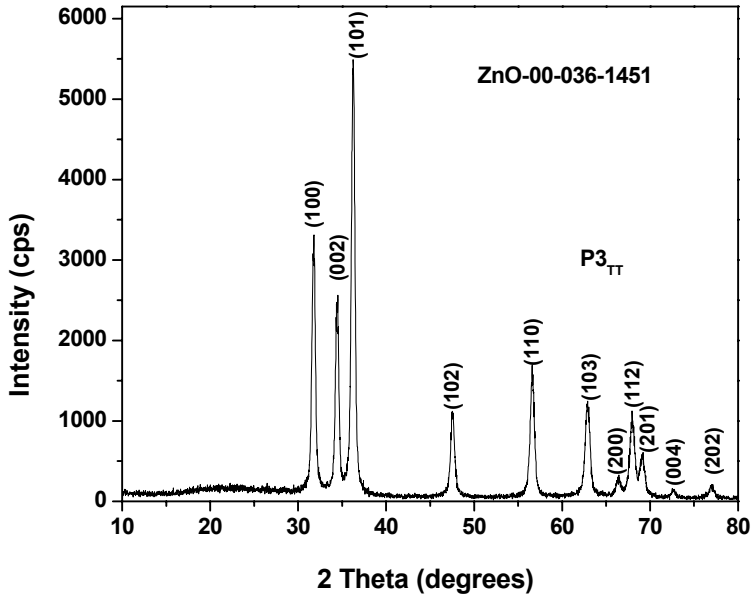

Fig. 5 – XRD pattern of the $P3_{TT}$ powder (P3 thermally treated at 300ºC for one hour).

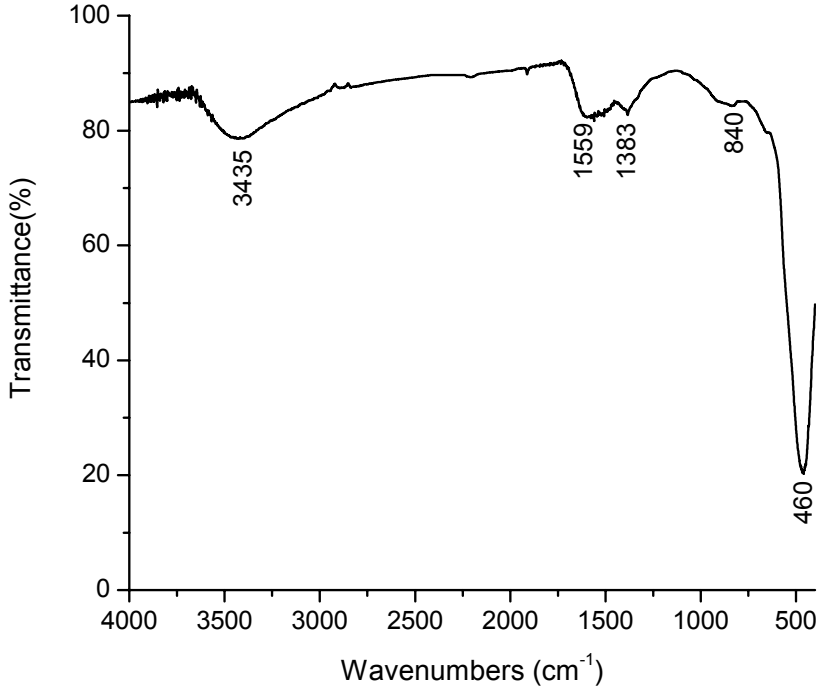

Fig. 6 – FTIR spectrum of the $P3_{TT}$ powder.

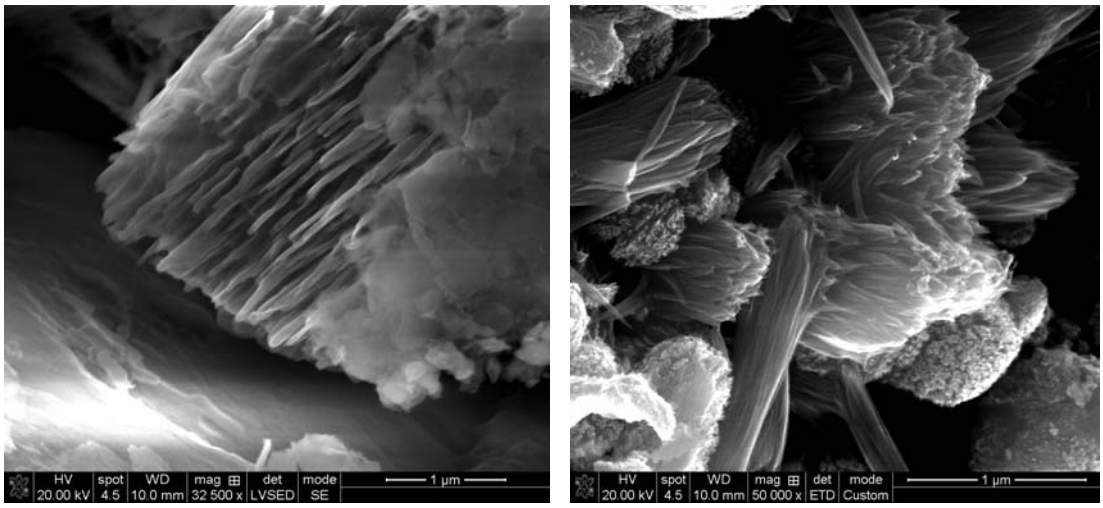

a) b)

Fig. 7 – SEM images of the P3 (a) and $P3_{TT}$ (b).

b) Powders obtained by hydrothermal method

The powders obtained in hydrothermal conditions $P_{HT\ unw}$ and $P_{HT\ w,}$ respectively, were investigated as-prepared and after washing the resulted powder with hot deionised water.

The comparative FTIR spectra of both powders are presented in Fig. 8. In the case of the as-prepared sample P_{HTunw} the bands at 3355, 1507 and 1045 cm^{-1} were attributed to stretching of O-H bonds. The band at 2929 cm^{-1} characteristic to the asymmetric stretching of CH_2 group, was observed also. The bands at 1384 and 832 cm^{-1} which appears in the spectrum were attributed to ν(NO) vibration mode. The bands below 744 cm^{-1} were characteristic to -Zn-O- vibrations.

In the FT-IR spectrum of P_{HTw} spectrum the intense band at 440 cm^{-1} was assigned to Zn-O vibration. The other small bands at 3125 cm^{-1} (hydrogen intramolecular bond), at 1615 cm^{-1} (H_2O vibration), at 1364, 1337 cm^{-1} (N-O asymmetric stretch) and 873 cm^{-1}(N-O symmetric stretch) were probably species absorbed on the surface of powder while in XRD only ZnO was observed.

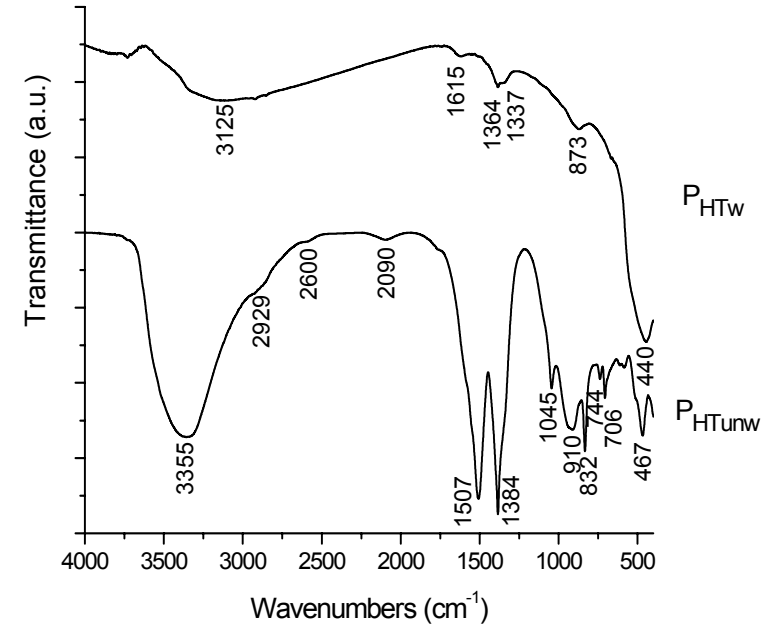

Fig. 8 – FTIR spectra of the P_{HTunw} and P_{HTw} samples.

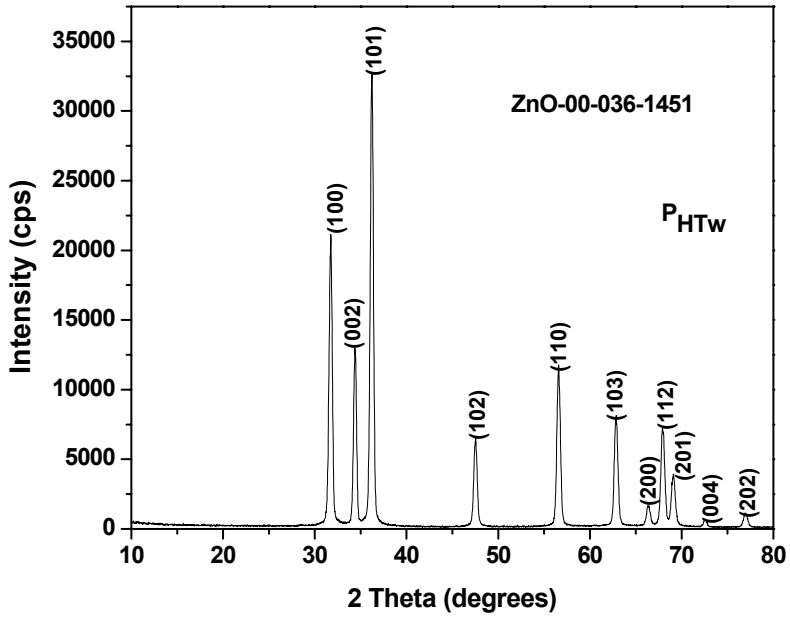

Fig. 9 – XRD pattern of the P_{HTw} sample.

The XRD pattern of the P_{HTw} sample synthesized through the hydrothermal method and washed by hot deionized water is presented in Fig. 9. The XRD pattern reveals that the as-synthesized product is the pure hexagonal wurtzite phase of ZnO which agrees well with the JCPDS card No.00-36-1451. The sharpness of the peaks implies a high crystallinity of the P_{HTw} sample. The lattice parameters of ZnO calculated from the diffraction data were a=b=3.2515 Å and c=5.2093Å respectively and the average crystallite size (D) 217 Å.

DSC analysis of the P_{HTunw} and P_{HTw} samples (Fig. 10) was also performed.

In the case of the P_{HTunw} sample an endothermic peak appears at 194°C which could be assigned to the decomposition of the ammonium nitrate (that remains in the as prepared powder).

For the P_{HTw} sample no peak is observed on the DSC curve. Correlated with FTIR spectrum and XRD pattern of the P_{HTw} sample, this result suggests that only zinc oxide phase is present in the powder that does not present any phase transformation in the temperature range investigated.

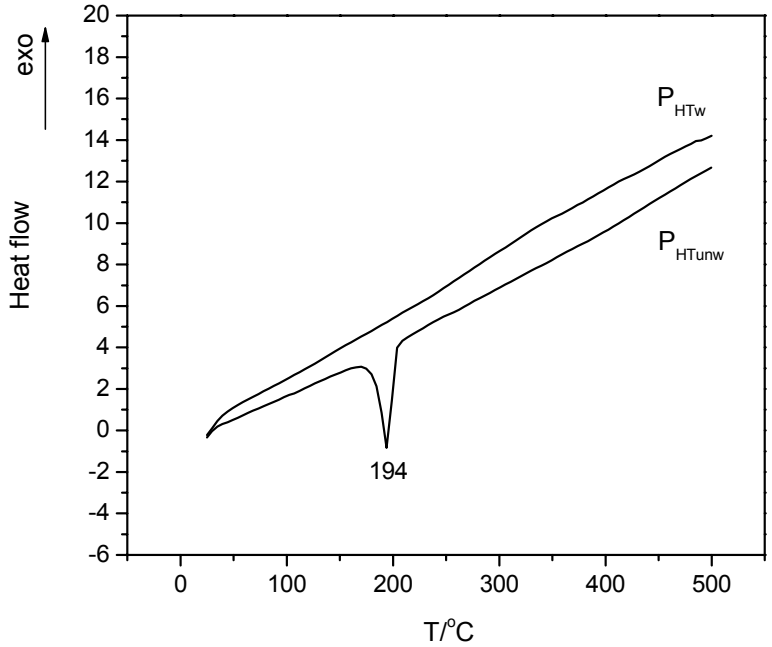

Fig. 10 – DSC curves of the P_{HTunw} and P_{HTw} samples.

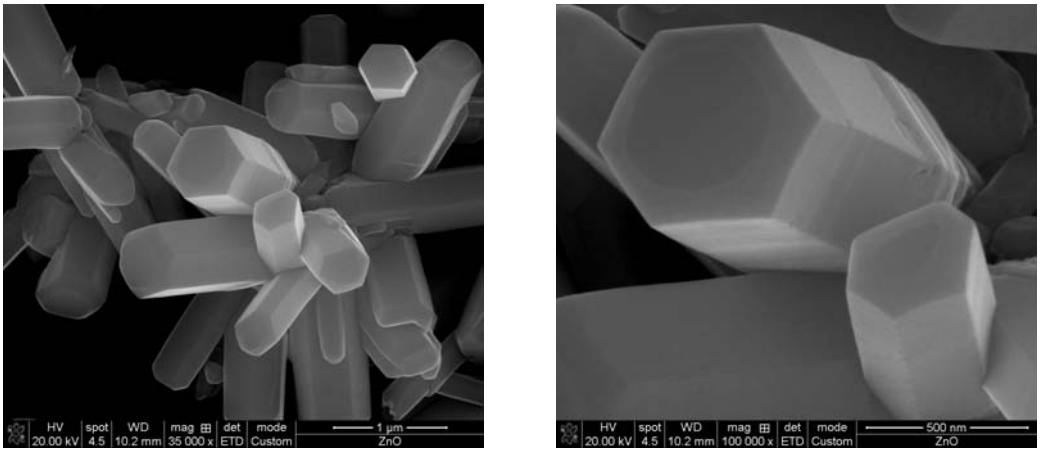

Fig. 11 – SEM images of the P_{HTw} sample.

The similarity between the FT-IR spectra of the powder obtained by hydrothermal method and washed with distilled water and of the powder P3 after thermal treatment at 300°C must be underlined.

The developed morphology of the P_{HTw} sample was observed in the Fig. 11 at different magnification grade.

It is highlighted that by the hydrothermal method, in our experimental conditions (with small content of HMTA), ZnO powder of well faceted hexagonal micro rods elongated along c-axis have been obtained.

CONCLUSIONS

Gels, precipitates and hydrothermal powder were obtained from the aqueous solutions in the $Zn(NO_3)_2.nH_2O$ (ZAH) - $(CH_2)_6N_4$ (HMTA) system depending on the experimental conditions.

The powders obtained from gels and precipitates consist of the mixture of phases. In the first case, the identified phases were: $Zn(OH)(NO_3).H_2O$ and NH_4NO_3 while in the case of the precipitate: $Zn_5(OH)_8(NO_3)_2.2H_2O$ and $Zn(OH)(NO_3).H_2O$ were identified. A good agreement between XRD and FTIR results was observed.

Their transformation of the as-prepared samples to ZnO was established by TG/DTA. Thermal decomposition takes place in three or two steps depending on the precursor powder, leading in all cases to the formation of ZnO powders at low temperature (300°C).

SEM images of the as prepared precipitates and thermally treated at 300 °C for one hour, show

similar blade-like nanostructure. This fact points out that initial blade–like structure is kept after thermal treatment.

By hydrothermal treatment of the $Zn(NO_3)_2.4H_2O$ (ZAH) - $(CH_2)_6N_4$ (HMTA) solution with 2:1 molar ratio ZnO nanorods were obtained. A higher crystalline degree was observed in the case of ZnO powder obtained by hydrothermal method than that obtained by chemical method and thermally treated at 300 °C for one hour.

Acknowledgements: This work was performed in the frame of interacademic cooperation with MTA-BME Technical Analytical Research Group of the Hungarian Academy of Science at the Budapest, Hungary and with a support of the EU (ERDF) and Romanian Government that allowed for acquisition of the research infrastructure under POS-CCE O 2.2.1 project INFRANANOCHEM - No. 19/01.03.2009. I. M. S. thanks for a János Bolyai Research Fellowship of the Hungarian Academy of Sciences. The authors also acknowledge the special support of Dr. Anca Braileanu with this cooperation.

REFERENCES

1. H. Gao, G. Fang, M. Wang, N. Liu, L. Yuan, C. Li, L. Ai, J. Zhang, C. Zhou, S. Wu and X. Zhao, *Mater. Res. Bull.,* **2008**, *43*, 3345-3351.
2. P. Uthirakumar, J.H. Kang and S. Senthilarasu, C.-H. Hong, *Physica E*, **2011**, *43*, 1746-1750.
3. L.-Y.Yang, S.-Y.Dong, J.-H. Sun, J.-L. Feng, Q.-H. Wu and S.-P.Sun, *J. Hazardous* Mat., 2**010**, *179*, 438-443.
4. C. Visinescu, F. Levy and V.I. Parvulescu, *Rev. Roum.Chim.*, **2006**, *51*, 827-833.
5. N.I. Ionescu and M. Căldăraru, *Rev. Roum. Chim.*, **2008**, *53*, 603-605.
6. N. I. Ionescu and M. Căldăraru, *Rev. Roum. Chim.*, **2010**, *55*, 365-367.
7. C.Baratto, G. Sberveglieri, A. Onischuk, B. Caruso and S. di Stasio, *Sens. Actuators*, *B*, **2004**, *100*, 261-265.
8. A.O. Dikovska, P.A. Atanasov, A.Andreev, B.S. Zafirova, E.I.Karakoleva and T.R Stoyanchov. *Appl Surf. Sci.*, **2007**, *254*, 1087-1090.
9. M.-K.Li, D.-Z.Wang , S.Ding, Y.-W. Ding, J. Liu and Z.-B. Liu, *Appl.Surf. Sci.*, **2007**, *253*, 4161-4165.
10. Z. Ben Ayadi, L. El Mir, K. Djessas and S. Alaya *Thin Solid Films*, **2011**, *519*, 7572-7574.
11. C. Pholnak, C.Sirisathitkul and D.J.Harding, *J.Phys. Chem. Solids*, **2011**, *72*, 817-823.
12. T. Krishnakumar, R. Jayaprakash, N. Pinna, V.N. Singh, B.R. Mehta and A.R. Phani, *Mater.Lett*., **2009**, *63*, 242-245.
13. V.R. Kumar, V.T. Kavitha, R.S. Wariar, S.U.K. Nair and J. Koshy, *J.Phys.Chem. Solids*, **2011**, *72*, 290-293.
14. T. Schuler and M.A. Aegerter, *Thin Solid Films*, **1999**, *351*, 125-131.
15. N. Rajeswari Yogamalar and A. Chandra Bose, *J. Solid State Chem.*, **2011**, *184*, 12-20.
16. S. Li, G.A. Gross, P.M. Günther and J.M. Köhler, *Chem.Eng.J.*, **2011**, *167*, 681-687.
17. S. Cimitan, S. Albonetti, L.Forni, F. Peri and D. Lazzari, *J. Coll. Interf. Sci.*, **2009**, *329*, 73-80.
18. N. Goswami and D.K.Sharma, *Physica E*, **2010**, *42*, 1675-1682.
19. C. K. Srikanth and P. Jeevanandam, *J.Alloys Compounds*, **2009**, *486*, 677-684.
20. O. Lupan, Th. Pauporte, I.M. Tiginyanu, V.V. Ursaki, H. Heinrich and L. Chow, *Mater. Sci. Eng B.*, **2011**, *176*, 1277-1284.
21. Q. Ahsanulhaq, S.H.Kim and Y.B.Hahn, *J. Phys. Chem. Solids*, **2009**, *70*, 627-631.
22. S. Anas, R.V. Mangalaraja and S. Ananthakumar, *J. Hazardous Mater.*, **2010**, *175*, 889-895.
23. D. Polsongkram, P. Chamninok, S. Pukird, L. Chowb, O. Lupan, G. Chai, H. Khallaf, S. Park and A. Schulte, *Physica B*, **2008**, *403*, 3713-3717.
24. P. Y. Wu, J. Pike, F. Zhang and S. W. Chan, *Int. J. Appl. Ceram. Technol.*, **2006**, *3*, 272-278.
25. B. Ribar, M.Šljukić, B.Matković, F.Gadela and E.Girt, *Acta Cryst.*, **1967**, *23*, 1113.
26. B. Małecka, R. Gajerski, A. Małecki, M. Wierzbicka and P. Olszewski, *Thermochim. Acta*, **2003**, *404*, 125-132.
27. J. Coates, "Interpretation of infrared spectra, a practical approach", Encyclopedia of Analytical Chemistry. Ed. Wiley and Sons, 2000, p.10815-10837.
28. A.T. Balaban, M. Banciu and I. Pogany, "Aplicaţii ale metodelor fizice în chimia organică", Ed. Ştiinţifică şi Enciclopedică, Bucureşti, 1983, p. 13-38.
29. T. Biswick, W. Jones, A. Pacula, E. Serwicka and J. Podobinski, *J. Solid State Chem.*, **2007**, *180*, 1171-1179.
30. G.V.Chertihin, *J. Chem Phys*., **1997**, *106*, 3457-3465.
31. J.P. Auffredic and D. Louër, *J. Solid State Chem*., **1983**, *46*, 245-252.